Toughening of Polylactide by Melt Blending with Methyl Methacrylate–Butadiene–Styrene Copolymer

Huiliang Zhang,[1] Nanan Liu,[1] Xianghai Ran,[1,2] Changyu Han,[1] Lijing Han,[1,2] Yugang Zhuang,[1] Lisong Dong[1]

[1]*State Key Laboratory of Polymer Physics and Chemistry, Changchun Institute of Applied Chemistry, Changchun 130022, China*
[2]*Graduate School, Chinese Academy of Sciences, Beijing 100080, China*

Received 29 March 2010; accepted 30 January 2012
DOI 10.1002/app.36952
Published online in Wiley Online Library (wileyonlinelibrary.com).

ABSTRACT: Brittle polylactide (PLA) was toughened by introducing 5–25 wt % of methyl methacrylate–butadiene–styrene (MBS) copolymer. PLA/MBS blends were characterized by dynamic mechanical analysis (DMA), differential scanning calorimetry (DSC), dynamic rheometer, mechanical testing, scanning electron microscopy, and transmission electron microscope. From the result of DSC, MBS could act as an effective heterogeneous nucleation agent for PLA and significantly improved the degree of crystallinity of PLA. DMA results showed a single high temperature peak of T_g between that of pure PLA and that of the shell composition of the MBS, which suggested that PLA and the shell of MBS were compatible. With an increase of MBS content, the tensile strength of the blends decreased; however, the elongation at break and impact strength increased significantly which indicated the toughening effects of the MBS on PLA. It was found that the PLA matrix showed large plastic deformation (shear yielding) in the blend subjected the impact tests, which was an important energy-dissipation process and led to a toughened polymer blend. MBS could act as impact modifier of PLA. Rheological investigation demonstrated that there was a significantly dependence of viscosity on composition. When the MBS content increased, the viscosity began to increase. J Appl Polym Sci 000: 000–000, 2012

Key words: polylactide; methyl methacrylate–butadiene–styrene; blends; toughening

INTRODUCTION

The growing global concern over persistent plastic waste has generated much interest in biodegradable polymers for everyday use. Biodegradable polymers based on polylactide (PLA) are one of the most attractive candidates as they can be readily produced from renewal agricultural sources such as corn. Recent developments in the manufacturing of the polymer economically from agricultural sources have accelerated the polymers emergence into the biodegradable plastic commodity market. Although the biodegradable aspects of PLA are important for the biomedical applications, the fact that it is derived from renewable resources makes it even more attractive from an environmental standpoint. PLA could foreseeingly become an alternative to traditional commodity plastics for everyday applications. Unfortunately, the broad substitution of commodity plastics by PLA is thwarted by its brittle behavior under impact loads.[1] However, because of its brittleness, wider applications of PLA to replace the nondegradable polystyrene and poly(vinyl chloride) are restricted.

Therefore, much work has been done to develop effective toughening methods for PLA.[2–11] An approach used successfully to strengthen or toughen brittle or stiff PLA is by incorporating a soft or elastomeric second component by blending. When the softer component forms a second phase within the more brittle continuous phase, it may act as a stress concentrator which enable ductile yield and prevents brittle failure.[12–15] It is well known that core-shell latex polymers are very effective toughening agents for polymers because the core size and shape can be controlled or designed when the core-shell latex polymer is synthesized. At the same time, the core is "locked in" by slight crosslinking and grafting with its shell to keep them from separating during mechanical blending.[16] Hence, a modified polymer with different mechanical properties may be

Correspondence to: L. Dong (dongls@ciac.jl.cn).
Contract grant sponsor: Science and Technology Bureau of Jilin Province of China; contract grant number: 20090320.
Contract grant sponsor: Ministry of Science and Technology of China; contract grant number: 2009GJB10042.
Contract grant sponsor: Chinese Science Academy (Changchun Branch); contract grant number: 2009SYHZ0028.

obtained using core-shell latex polymer with cores of different sizes and/or morphology. On the other hand, the adhesion between the two phase, core-shell latex polymer and polymer matrix, depends strongly on the degree of miscibility of the shell of the core-shell latex polymer with the matrix, that is, whether they are completely miscible, partially miscible, or immiscible. However, complete miscibility is not always necessary for blends for different applications. On the contrary, in some cases, partial miscibility of the components is used to obtain blends of desired properties (e.g., impact-modified blend).[17,18]

Core-shell modifiers are used regularly to improve the toughness of the polymer matrix due to three major attractive features: (1) the rubbery core provides resistance to impact, especially at low temperature, whereas the grafted glassy shell provides rigidity and compatibility to the polymer matrix, keeping the particles desired shape and dispersibility; (2) the rubber particle diameter, particle diameter distribution, crosslink density, grafting degree, shell thickness, shell composition, and overall composition, can be individually studied and optimized.

PLA materials fail in a brittle manner under certain loading conditions such as notched Izod impact test. PLA has been blended with several polymers to modify its properties,[19,20] but no work has been done on PLA/methyl methacrylate–butadiene–styrene (MBS) blends. Zhang et al. have studied that PLA/polymethyl methacrylate (PMMA) blends was a miscible blend.[21] MBS has a soft core (butadiene–styrene copolymer) and a hard shell (PMMA). It is often used as an impact modifier of PVC because of its high stiffness, high modulus, and good miscibility with PVC.[22–25]

In this study, PLA was blended with MBS and its miscibility, phase behavior, crystallization behavior, and rheological behavior were investigated. From the analysis of dynamic mechanical analysis (DMA), PLA is compatible with the PMMA shell of MBS. The brittle-ductile transition phenomenon was observed. This work aims at assessing the miscibility, phase morphology, and the toughening mechanisms of PLA/MBS blends.

EXPERIMENTAL

Material and blend preparation

Semi-crystalline PLA Grade 2002 D (4% D-lactide, 96% L-lactide content, molecular weight 121,400 g/mol, melt flowing rate (MFR) 6.4 g/10 min) was obtained from Natureworks™ in pellet form. MBS, trademark: B-521, was purchased from Kaneka Corporation, Japan.

PLA and MBS were dried at 70°C for 8 h in a vacuum oven. PLA/MBS blends were prepared by melt mixing with a Haake Rheomix 600 (Karlsruhe, Germany) at a rotating speed 60 rpm at 180°C for 5 min. The mixing compositions of the PLA/MBS blends were 95/5, 93/7, 90/10, 85/15, 80/20, and 75/25 w/w. Also, the neat PLA was subjected to the same mixing treatment to create the same thermal history as that of the blends. After mixing, all of the compounds were cut into small pieces. Then, all of samples were compression-molded into sheets with thicknesses of 1.0 and 6.35 mm at 185°C for various tests. The hydraulic press was set at 120 kg/cm^2.

Characterization

Notched Izod impact tests were performed at 23°C ± 2°C according to ASTM D256-2010 on an impact testing machine (CEAST, Chengde, China). The samples with dimensions 63.5 × 12.7 × 6.35 mm^3 were obtained from compression-molded specimens. The notch was milled in having a depth of 2.54 mm, an angle of 45°, and a notch radius of 0.25 mm. The uniaxial tensile tests were carried out at 23°C ± 2°C on an Instron 1121 testing machine (Canton MA). Specimens (20 × 4 × 1 mm^3) were cut from the previously compression-molded sheet into a dumbbell shape. The measurements were conducted at a cross-head speed of 50 mm/min at room temperature according to ASTM D638-2008. At least five runs for each sample were measured, and the results were averaged.

DMA was performed on a NETZSCH DMA 242C (Selb, Germany), which provided the plots of the loss tangent (tan δ) and the storage modules (E') against temperature. The samples were sized 20 × 4 × 1 mm^3. The experimental was carried out in tension mode at a constant heating rate of 3°C/min and a frequency of 3.33 Hz, from −120°C to 150°C.

Crystallization behavior of the composites was studied by differential scanning calorimetry (DSC) (TA Instruments DSC Q20 USA) on the specimens sliced from compression molded samples. The heating and cooling rates were 10°C/min with nitrogen purge, and the sample weights were between 8 and 10 mg. The samples were heated first from 20°C up to 180°C at 10°C/min and held at 180°C for 5 min to eliminate their previous thermal history, then cooled at the same rate, and heated again finally. The absolute degree of crystallinity [$X(t)$] of the samples was evaluated from the heat evolved during crystallization by the following relationship:

$$X(t) = \left[\int_{t_0}^{t} (dH/dt)\right] / (1 - \Phi)\Delta H_f^0 \qquad (1)$$

where ΔH_f^0 is the heat of fusion for 100% crystalline PLA (93 J/g)[26] and Φ is the weight fraction of MBS in the blend system.

Rheological measurements of the blends were conducted with a Physica MCR 2000 rheometer (AR

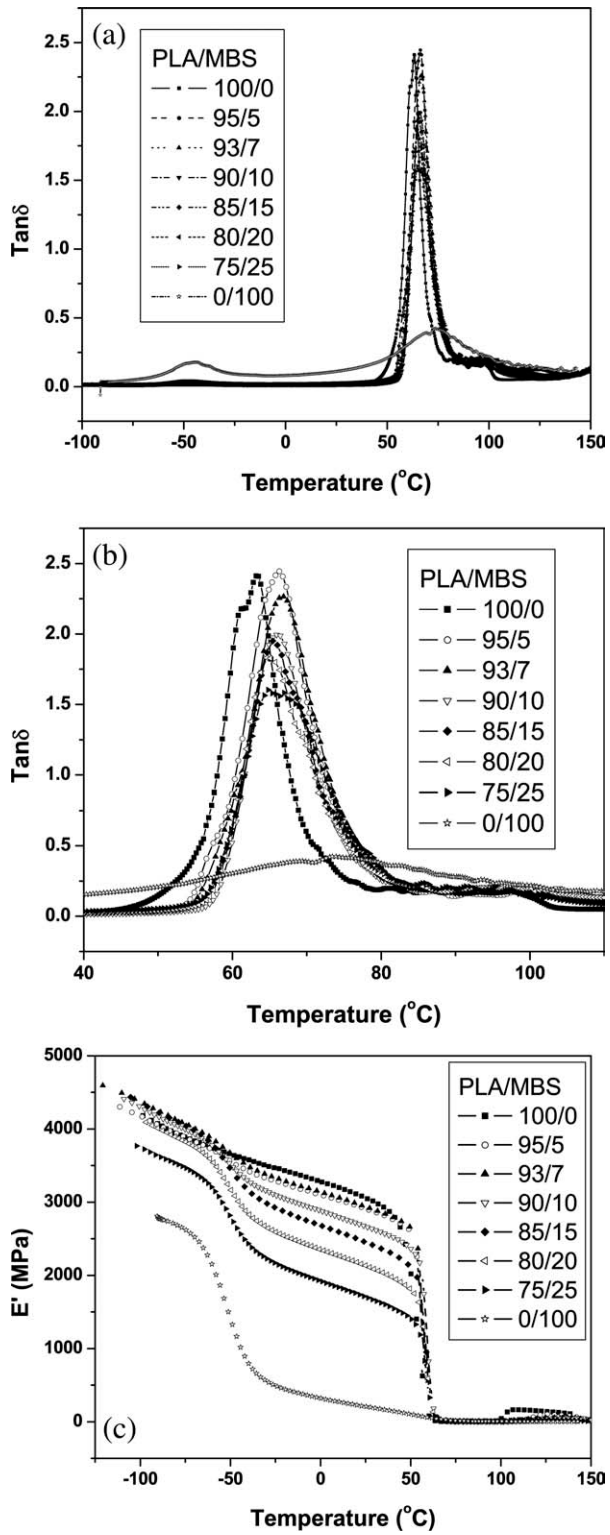

Figure 1 Dynamic mechanical properties of PLA/MBS blends: (a) tan δ, (b) tan δ (40–110°C), and (c) the storage modulus (E').

2000ex USA) at 200°C. Frequency sweep for the PLA/MBS samples was carried out under nitrogen using 25-mm plate-plate geometry. The gap distance between the parallel plates was 0.8 mm for all tests. The sheet samples were about 1.0 mm in thickness. A strain sweep test was initially conducted to determine the linear viscoelastic region of the materials. The angular frequency range used during testing was 0.1–100 rad/s.

The fracture surfaces of PLA/MBS blends from the impact and tensile tests were characterized by scanning electron microscopy (SEM) (model Japan JXA-840 ESEMFE). A layer of gold was sputter-coated uniformly over all of the fractured surfaces before SEM observations.

Transmission electron microscope (TEM) samples were microtomed in stress-whitening zone of impact specimens to examine the deformation behavior immediately underneath the fracture surface. The ultrathin sections were parallel to the deformation direction. The specimens were cut to 60 nm in thickness using a microtome at −100°C. The samples were collected on 200-mesh copper grids and stained by exposing the ultrathin sections in the vapor of 1%

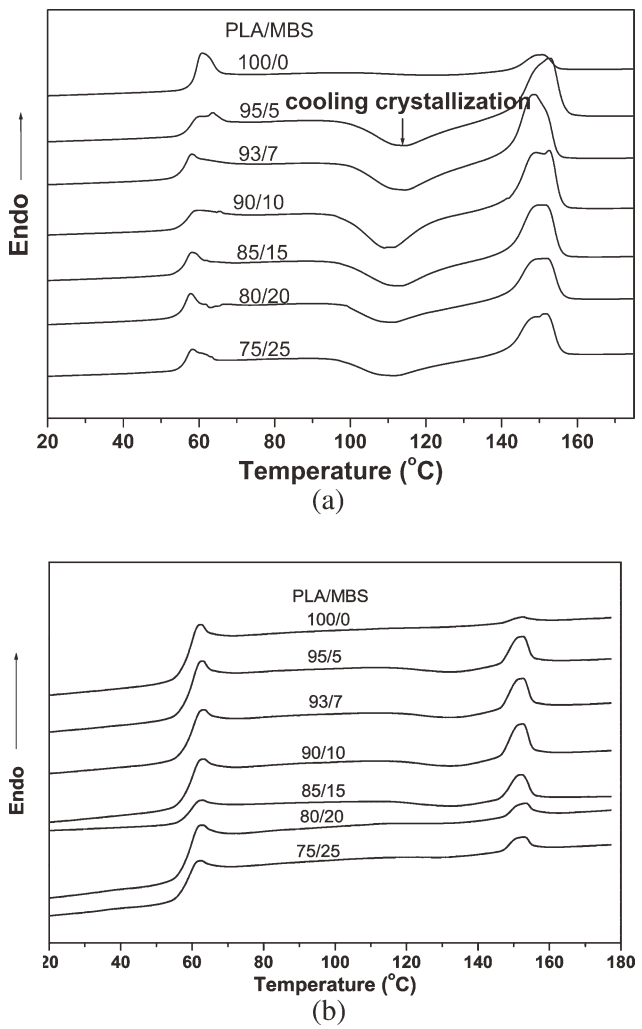

Figure 2 DSC thermograms for PLA/MBS blends with compositions from 100/0 to 75/25: (a) in the first heating runs and (b) in the second heating runs.

TABLE I
Crystallization Properties of PLA/MBS Blends

	First heating run					Second heating run			
PLA/MBS (w/w)	T_g (°C)	T_m (°C)	T_{cc} (°C)	ΔH_f (J/g)	X_c (%)	T_g (°C)	T_m (°C)	ΔH_f (J/g)	X_c (%)
100/0	59.3	150.6	122.4	5.75	6.2	58.6	152.3	1.08	1.2
95/5	58.2	153.1	113.8	24.39	27.6	58.6	152.6	3.29	3.7
93/7	56.6	148.4	113.1	25.95	30.0	58.9	152.4	3.42	4.0
90/10	57.0	152.8	110.6	28.95	34.6	58.6	152.4	3.59	4.3
85/15	56.7	151.6	112.4	23.46	29.6	58.7	152.3	3.15	4.0
80/20	56.2	151.8	110.8	20.02	26.9	59.0	152.7	1.63	2.2
75/25	57.0	151.8	110.8	18.14	26.0	58.7	152.7	1.42	2.0

ΔH_f of PLA is 93 J/g.

OsO_4 solution for 8 h before observation. A TEM (model Japan JEM-2000 EX) operated at 124 kV was used to study the deformation mechanisms.

RESULTS AND DISCUSSION

Miscibility

Figure 1(a–c) shows the dependence of loss factor (tan δ) and storage modulus (E') on the temperature for PLA modified with different contents of MBS, respectively. In Figure 1(a,b), the core-shell MBS particle contains one core portion which is a butadiene–styrene copolymer having a T_g of −45.0°C, and one shell portion that has a broad loss peak of 74.2°C. The broadening of loss peak implies that the shell portion is a mixture of different material. MBS core-shell particles are made by sequential polymerization, so it is possible that some residual butadiene monomer left over from making the core was copolymerized with methyl methacrylate, and the composition of the random copolymer being formed in this way altered as the butadiene was used up, giving a mixture of copolymers with a range of T_g's. In Figure 1(b), pure PLA shows a single peak of T_g (62.8°C), the PLA/MBS blends showed a single high temperature peak of T_g between that of pure PLA and that of the shell composition of the MBS, which suggested that some high-T_g component of the MBS additive is sufficiently miscible with PLA to raise its T_g. Compatibility between PLA and the shell composition of the MBS is very important for achieving good ultimate mechanical properties, because it enhances the phase interfacial adhesion.

In Figure 1(c), neat PLA showed a gradual decrease of E' with an increase of temperature from −100 to 50°C and then dropped rapidly because of the glass transition and reached a minimal value around 75°C. By further increasing the temperature, E' increased and achieved a maximal value around 105°C. This reflected an enhancement of the sample rigidity resulting from the cold crystallization process detected by the DSC. Above 105°C, the E' dropped again. One possibility is a reduction in pressure from the grips of the tensile machine as a result of shrinkage during cold crystallization. The influence of the MBS on E' curve depended on the temperature region. Below the glass transition temperature of butadiene–styrene copolymer (T_g −45°C), the storage modulus of 93/7, 90/10, 85/15, and 80/20 PLA/MBS blends are within the same order as the pure PLA and the E' of 75/25 PLA/MBS is much lower that of the pure PLA. On the contrary, above −45°C, E' of PLA/MBS samples decreased rapidly and reached minimal values located at temperature range (60–80°C) as compared with neat PLA, which indicated that the rigidity of the blends decreased. The result was attributed to the increase in the segmental mobility of the butadiene–styrene chains. Then, E' of 75/25 PLA/MBS

TABLE II
Mechanical Properties of PLA/MBS Blends

PLA/MBS	Tensile strength (MPa)	Elongation at break (%)	Young's modulus (MPa)	Izod impact Strength (kJ/m^2)
100/0	69.8 ± 3.2	5.7 ± 0.3	1777 ± 42	4.7 ± 0.2
95/5	63.3 ± 2.5	20.7 ± 1.9	1212 ± 45	5.5 ± 0.3
93/7	54.3 ± 2.1	310 ± 30	1189 ± 37	6.0 ± 0.3
90/10	44.5 ± 1.9	380 ± 22	1120 ± 35	12.6 ± 2.6
85/15	42.7 ± 2.3	360 ± 26	1080 ± 39	44.7 ± 4.4
80/20	38.1 ± 1.4	334 ± 21	753 ± 32	83.1 ± 0.2
75/25	33.9 ± 1.7	300 ± 18	718 ± 27	97.2 ± 3.4
0/100	7.0 ± 0.4	200 ± 13	101 ± 19	

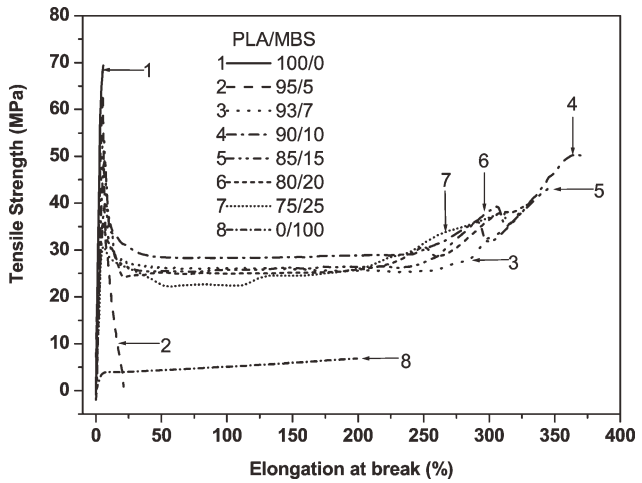

Figure 3 Tensile behavior of PLA/MBS blends: (1) 100/0, (2) 95/5, (3) 93/7, (4) 90/10, (5) 85/15, (6) 80/20, (7) 75/25, and (8) 0/100.

increased because of the cold crystallization process in the temperature region characteristic for the neat PLA. Above 100°C, it decreased finally.

Thermal properties

The DSC heating thermograms shown in Figure 2(a,b) exhibited three main transitions successively: a glass transition, a cold crystallization exotherm, and a melting endotherm. The measured values of the phase-transition parameters were summarized in Table I.

In Figure 2(a), neat PLA displayed a broad cold crystallization exotherm at 122°C during the first run, approximately. The incorporation of MBS decreased cold crystallization temperature by $\sim$ 13°C and narrowed the peak width, indicating an enhanced crystalline ability of PLA. This could be explained that the MBS particles acted as nucleation centres and promoted the crystallization of PLA. Thus, the cold crystallization temperature moved to a lower temperature. Double melting peaks appeared at about 148.4 and 151.8°C in the PLA/MBS blends. The addition of MBS clearly separated the melting peak of neat PLA into two individual peaks. The peaks at higher temperatures correspond to the shoulder of the neat PLA. The peaks at lower temperatures were $\sim$ 3.6°C lower than the peak of neat PLA (Table I). This bimodal melting peak was induced during the moulding-press process when the less perfect crystals had enough time to melt and reorganize into crystals with higher structural perfection and remelt at higher temperature.[27,28]

In Figure 2(b), in the second heating run, the glass transition temperatures (T_g's) of PLA/MBS blends were independent with the increase of MBS content in the blends. The cold crystallization exotherms during the second heating run were smaller than those of the first heating run.

From the Table I, in the first heating run and the second heating run, the absolute degrees of crystallinity of 95/5, 93/7, 90/10 PLA/MBS blends increased continuously with the increase of MBS content in the blends, the dispersive particles of MBS could be acted as heterogeneous nucleation agent and increased the degrees of crystallinity of 95/5, 93/7, 90/10 PLA/MBS blends. A sufficient amount of agglomeration of the MBS particles became partially continuous phase, whereas the content of MBS composition was up to 15%, the degrees of crystallinity of 85/15, 80/20, and 75/25 PLA/MBS blends were restricted by amorphous MBS and began to decrease.

Mechanical properties

The tensile properties of PLA/MBS blends were given in Table II. The addition of MBS changed the tensile behavior of the PLA significantly, as was shown in Figure 3. The brittle fracture of the neat PLA transformed to ductile fracture for the PLA/MBS blends when the materials subjected to tensile testing. Neat PLA is very rigid and brittle. The tensile strength is 69.8 MPa and the elongation at break is only about 5.7%. It showed brittle fracture upon the tensile load. In contrast, all of the PLA/MBS blends showed clear yielding behavior upon stretching. After yielding occurred, the strain developed continuously, whereas the stress remained constant almost and the samples broke finally with a high elongation compared with that of the neat PLA. It was very interesting to find that the 85/15 PLA/MBS blend had a very high elongation at break of 360%, whereas the tensile strength remained as high as 42.7 MPa (Table II). Moreover, the elongation at

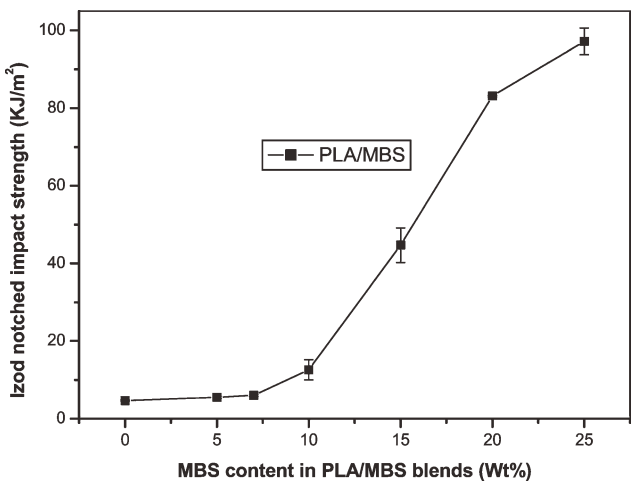

Figure 4 Notched impact strength of PLA/MBS blends with different MBS content.

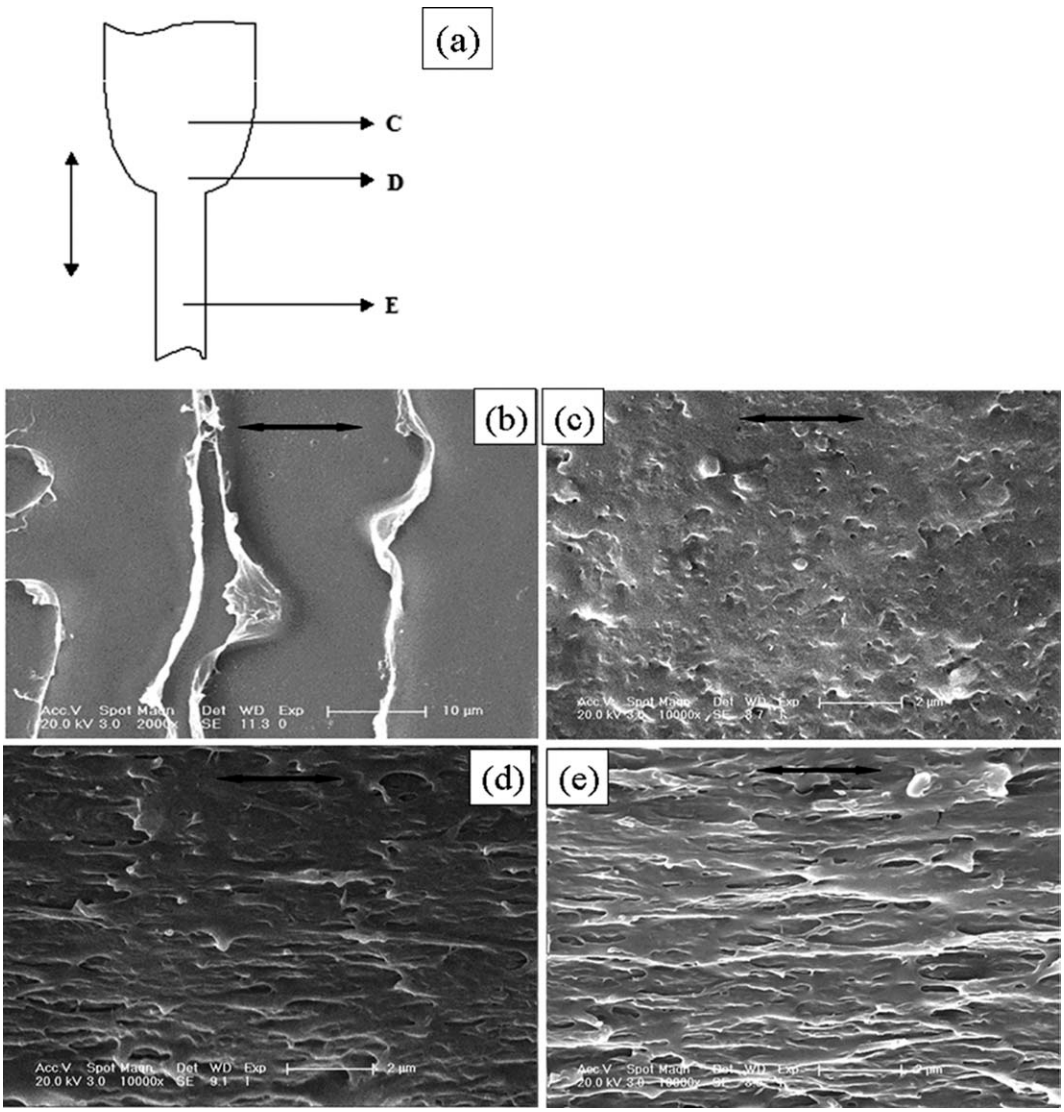

Figure 5 (a) Schematic diagram of the measurement locations C, D, and E of the SEM micrographs of PLA/MBS 80/20 blend during tensile testing. (b) Neat PLA, (c) morphology in region C, (d) morphology in region D, and (e) morphology in region E. The arrow indicates the stretching direction.

break decreased slightly with the increase of MBS content. On the other hand, the tensile strength (Fig. 3) and the modulus decreased with the addition of MBS, which was due to the lower modulus and tensile strength of MBS than those of PLA.

From Figure 4, the impact strength of the PLA/MBS blends was measured for various MBS contents. The impact strength was significantly changed from 4.7 kJ/m^2 for neat PLA to 97.2 kJ/m^2 for the PLA/MBS 75/25 blend. The brittle-ductile transition of the blends was obtained when the MBS contents varied from 10% to 15%.

To study the toughening mechanism of PLA/MBS blends, the necked down region of the tensile specimen was cryo-fractured longitudinally. SEM micrographs of fractured surfaces are shown in Figure 5. The micrographs of the tensile specimen were taken at different locations of the necked down region as depicted in Figure 5(a), where the stress state varied. Neat PLA which had no necking in the tensile test showed a smooth longitudinal fracture surface without visible plastic deformation in Figure 5(b). In Figure 5(c–e), oval cavities are visible near the necked down region of the PLA/MBS blends during tension where dilating stresses were created. These cavities were formed when the volumetric strain energy released by forming a void is greater than the surface energy needed to form new surface plus the energy needed to stretch the surrounding rubber to make space for the void.[29] These cavities were enlarged in the stress direction along with the deformation of the matrix. Because of the cavitation formed in the MBS particles, the stress whitening is caused by the light scattering. Cavitation is

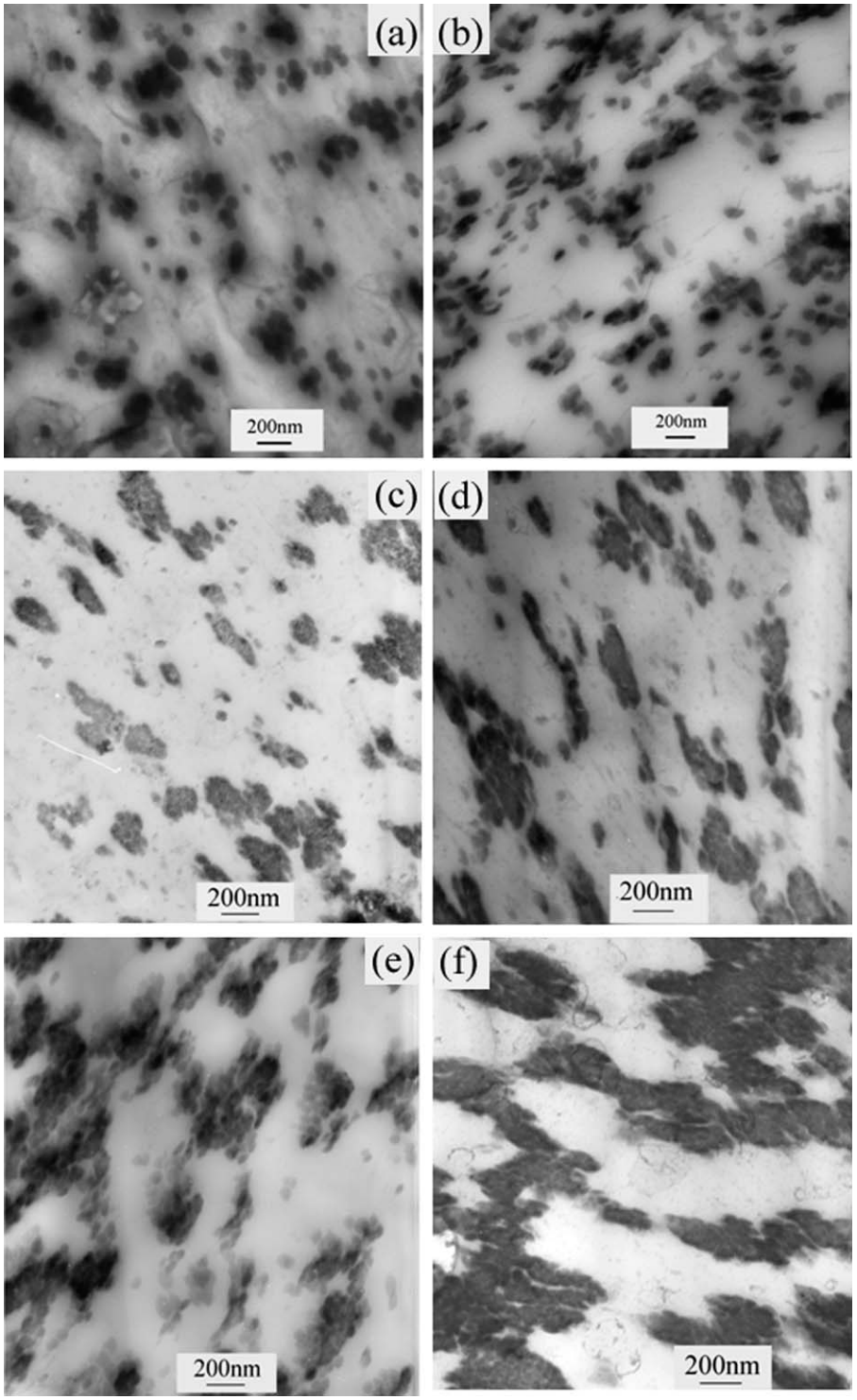

Figure 6 TEM morphology in the deformed zone of PLA/MBS blends: (a) 95/5, (b) 93/7, (c) 90/10, (d) 85/15, (e) 80/20, and (f) 75/25.

important in notched specimens because it enables the blend to yield at moderate stresses under plane strain conditions.[30,31]

Deformed morphology inside the fracture zone of PLA/MBS blends was shown in Figure 6. The MBS particles (the black domain dispersing in the matrix) were elongated remarkably and obvious deformation of MBS particles could be seen, which indicated shear yielding was the major energy absorbance way. Only a limited number of the original particles still existed, MBS particles were mainly 60–70 nm in diameter aggregated to form clusters and the size of clusters was increased with increasing MBS content. For the 90/10 PLA/MBS blend, the MBS particles

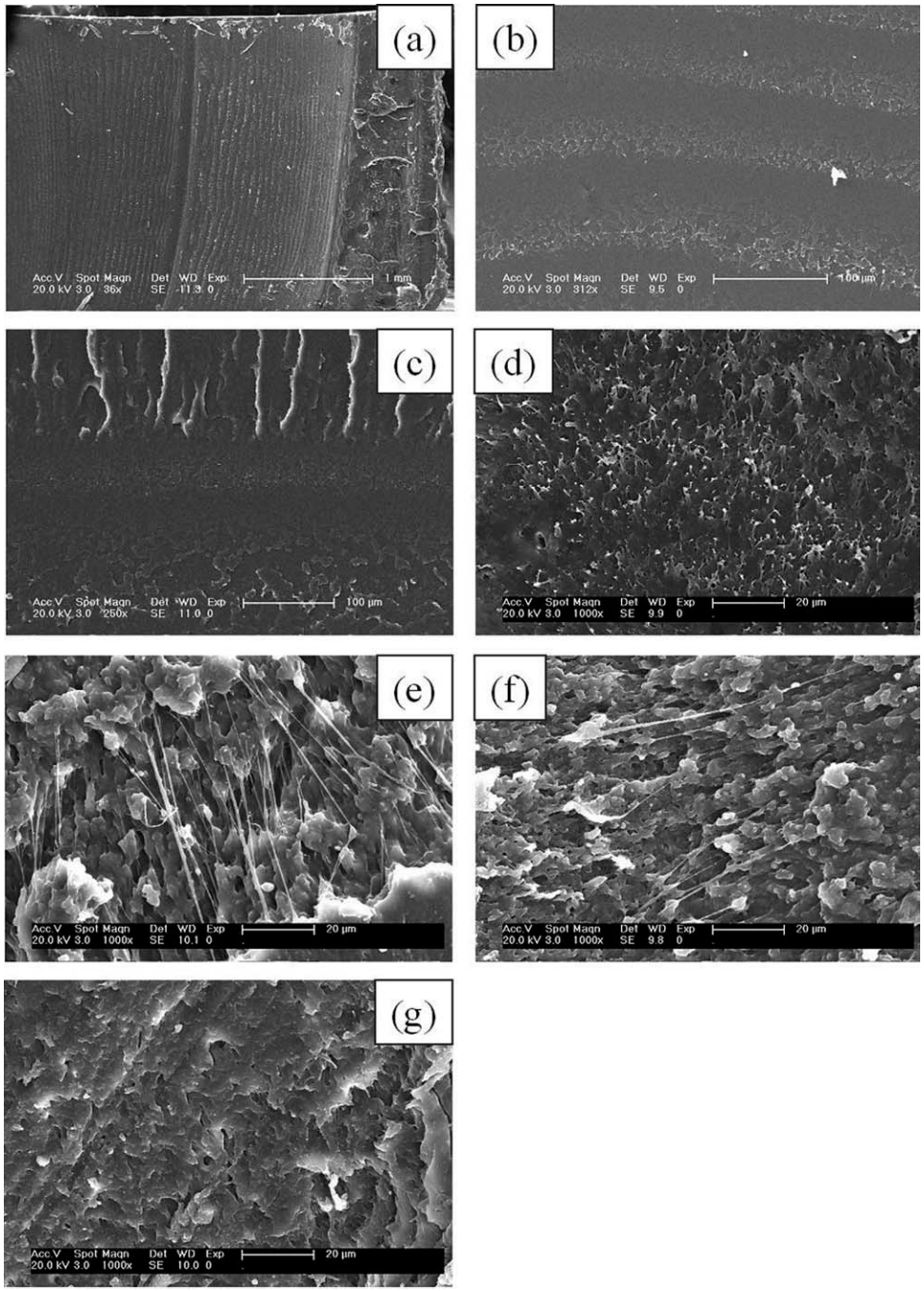

Figure 7 SEM photographs of the impact fracture surface of PLA/MBS blends: (a) 100/0, (b) 95/5, (c) 93/7, (d) 90/10, (e) 85/15, (f) 80/20, and (g) 75/25.

were elongated, which could be attributable to the shear yielding of PLA matrix. On comparison with the 90/10 PLA/MBS blend, the 85/15, 80/20 PLA/MBS blends showed similar phase morphology except that the concentration of dispersed particles was increased. As for the 75/25 PLA/MBS blend, the agglomeration of the dispersed phase gave rises to a nearly co-continuous structure. The yielding process can then propagate and pervade over the entire deformation zone. They also showed the same phenomenon in PBT/AES blends.[32]

The photographs of the impact fracture surface of PLA/MBS blends can be observed by using SEM. As could be seen from Figure 7(a–c), the fracture surface of 100/0, 95/5, and 93/7 PLA/MBS blends showed relatively smooth, indicating that little plastic deformation had taken place during the impact test. This was in good agreement with their lower impact strength. From Figure 7(d–f), the fracture surface of 90/10, 85/15, and 80/20 PLA/MBS blends were rough and had many root-like whiskers and many long stretches of the ligaments, which

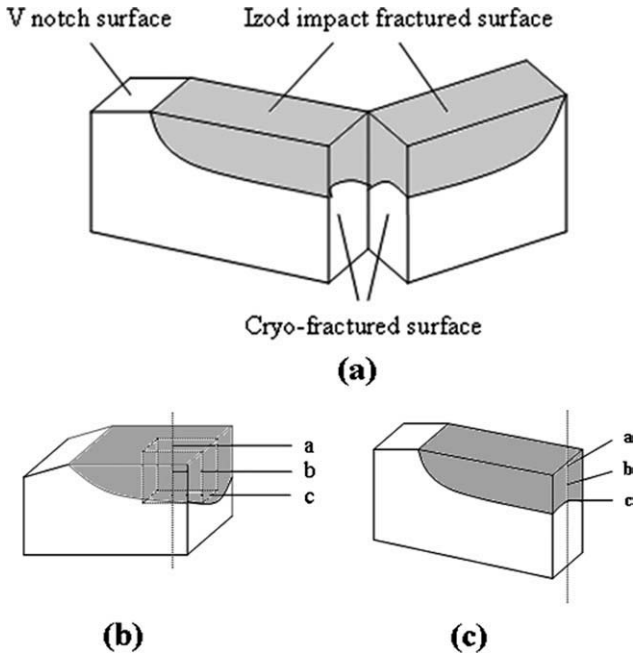

Figure 8 Schematic presentation of the preparation of samples used for examination of deformation mechanisms in PLA/MBS blends by using SEM. The gray areas represent the deformation region.

suggested that the impact specimen broke yieldingly. Wu et al. have studied that PVC/MB blends appeared such root-like whiskers.[33] Some fibrils could be observed for the PLA/MBS blends and the number of fibrils increased with the increase of MBS content. Such fibril-like structures have been reported in other rubber modified polymers.[34–37] For the 85/15, 80/20, and 75/25 PLA/MBS blends, the impact caused not only the fibrils but also some cavitations and a clear matrix deformation. In Figure 7(d–g), cavitation can be clearly identified. The large voids might be formed by the coalescence of neighboring small cavities. Figure 7(g) displayed the ductile fracture on which rumpled surface could be seen. The rumples lied parallel to the notch and gave rise to tufts of highly drawn material. The rumples had been explained as being due to considerable drawing ahead of the crack tip before unstable fracture sets in. The extensive deformation ahead of the crack tip gave rise to these structures. In particular, extensive plastic deformation of the PLA matrix could be observed clearly, which implied that shear yielding of the PLA matrix had taken place. It was a typical feature of a ductile fracture.

In order to correlate the external morphology of the ductile fracture surface to the internal deformation mechanisms of the yielded zone, the 80/20 PLA/MBS blend was chosen for SEM analysis. The 80/20 PLA/MBS blend was chosen for SEM analysis. Figure 8 provided schematic preparation of samples used for examination of deformation mechanisms in PLA/MBS blends by using SEM. The gray areas represent the deformation region. A number of scanning electron micrographs were obtained through the stress whitening zone of the sample as defined in Figure 8, and the sections were taken at different distances from the fracture surface. The surfaces parallel to the notched impact fractured surface were cut at low temperature with a glass knife until a smooth surface was obtained [Fig. 8(b)]. To observe the cryo-fractured surface, a

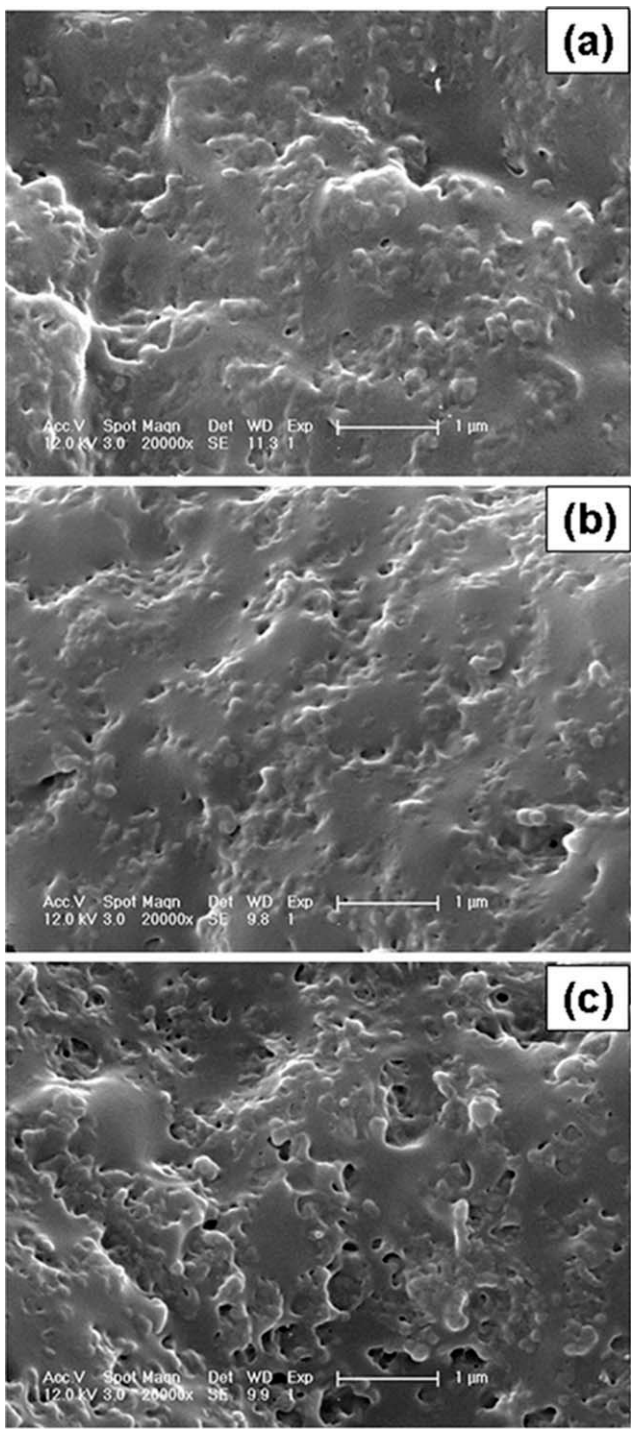

Figure 9 SEM micrographs in the deformation zone of PLA/MBS 80/20 blend. The location of the observed surfaces is illustrated in Figure 8(b).

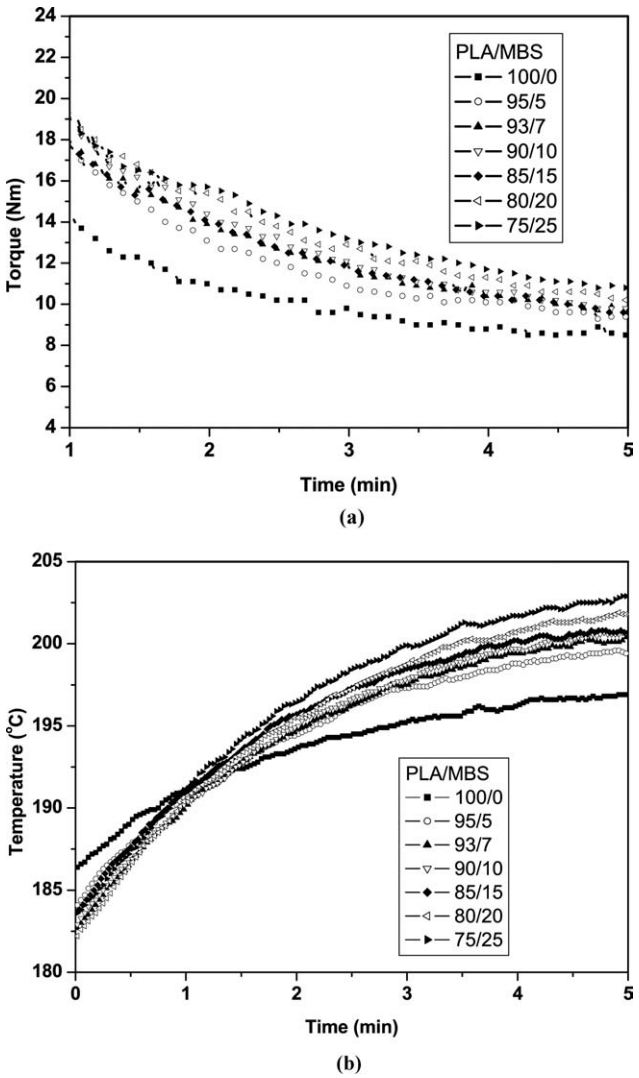

Figure 10 (a) The relation between the actual torque in the Thermo Haake mixer and mixing time for PLA and PLA/MBS blends. (b) The relation between the actual temperature in the Thermo Haake mixer and mixing time for PLA and PLA/MBS blends.

saw cut was prepared vertical to the fracture surface only 1 mm away from the stress whitening zone of the broken Izod impact specimen, and the saw cut was sharpened. Then, the specimen was immerged in liquid nitrogen for 3 h and torn open immediately; in this way, the cryo-fractured surface was prepared for investigation of inner morphology [Fig. 8(c)].

From Figure 9, we can find, in the surfaces parallel to the notched Izod impact surface, the small holes resulting from voiding of the rubber particles was observed. The voids increase in size with their position nearer the fracture surface [Fig. 9(a)].

Rheological properties

Figure 10(a) illustrates the evolution of the torque as a function of the mixing time for PLA/MBS blends.

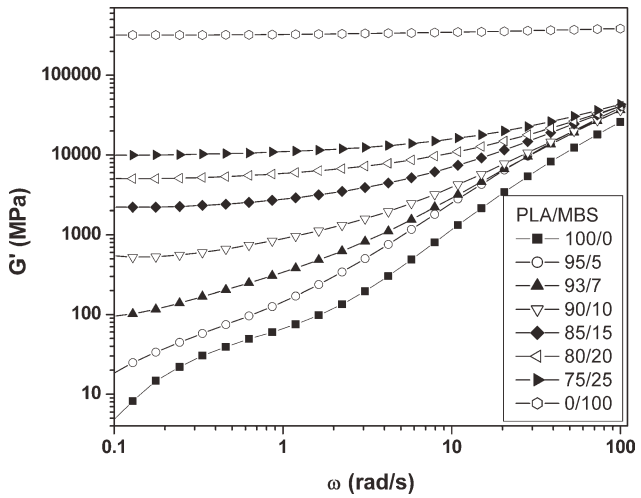

Figure 11 Plots of storage modulus versus angular frequency for the PLA and PLA/MBS blends.

It can be seen from Figure 10(a), compared with PLA, PLA/MBS has higher torque value. For the PLA/MBS blends, with the increase in MBS content in PLA/MBS blends, the torque values of the blends increase, which identifies the effect of the MBS viscosity.

Figure 10(b) illustrates the relation between the actual temperature in the Thermo Haake mixer and mixing time for PLA/MBS blends. The temperature increases with the mixing time increasing. Although the MBS content increases, the temperature in the mixer gets higher. It reaches about 203°C for the 75/25 PLA/MBS blend, the cause of heating is the visco-elastic behavior of the blend and the application of varying stresses during compounding. The torque values of all the blends fall because viscosity decreases with increasing temperature.

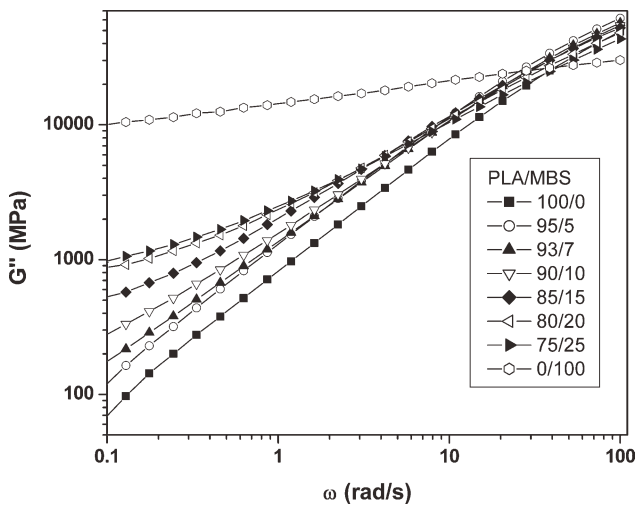

Figure 12 Plots of loss modulus versus angular frequency for the PLA and PLA/MBS blends.

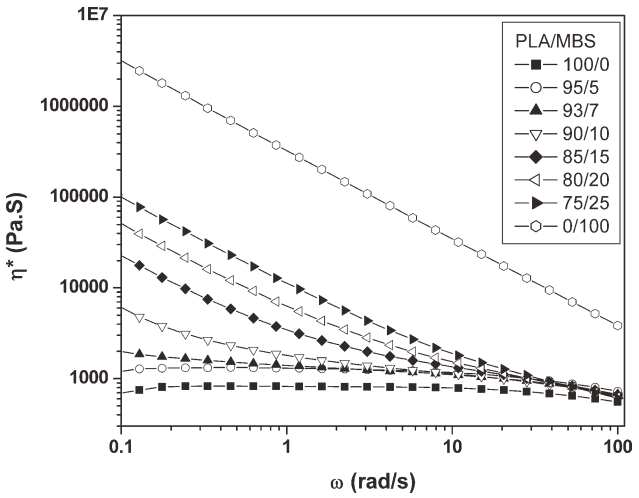

Figure 13 Plots of complex viscosity versus angular frequency for the PLA and PLA/MBS blends.

The dynamic rheological experiments were carried out for the PLA/MBS blends with the whole compositions. In Figure 11, it could be seen that the dynamic storage modulus G' of PLA/MBS blends increased with angular frequency and also increased with the increase of MBS content in the blends. At low frequencies, compared with that of the PLA matrix, the storage modulus of the 75/25 PLA/MBS blend increased by about 3 order. The higher absolute values of dynamic modulus indicated the formation of entanglement structures between the PLA chains and the grafted shell polymer chains of MBS.

Figure 12 displays the relationship between loss modulus and angular frequency of the PLA/MBS blends at 200°C. At low frequencies, the loss modulus of PLA/MBS was much higher than that of PLA. The much higher loss modulus indicated higher viscosity. At medium and high frequencies, the loss modulus of PLA/MBS was much lower than that of the neat PLA. This could be explained that the entanglement structure was formed at low frequencies and it was disentangled at high frequencies.

Figure 13 displayed the relationship between complex viscosity η* and angular frequency of the PLA/MBS blends at 200°C. The addition of MBS resulted in the gradual increase in the viscosity of the blends. It also appeared that PLA had a longer Newtonian region than those of PLA/MBS blends. In Figure 13, at low frequencies, the η* of the PLA/MBS blends were much higher than that of PLA due to viscosity dramatically increased.

The increase in viscosity and elasticity of the PLA/MBS blends compared with PLA at low shear rate range can be attributed to the increase of the interfacial adhesion between MBS and PLA, caused by the formation of entanglements between PLA chains and the grafted shell chains of MBS. The toughening effect was attributed to the energy dissipation caused by these tiny core-shell structure MBS particles having strong interfacial adhesion between the shell of MBS and the PLA matrix.

CONCLUSIONS

1. From the analysis of DMA, PLA were compatible with the shell of MBS.
2. The mechanical properties of PLA could be improved by the addition of 5–25% MBS. The elongation at break as well as impact strength of PLA/MBS blends was improved significantly compared with neat PLA. The impact strength of the 75/25 PLA/MBS blend was about 21 times the impact strength of pure PLA.
3. From SEM micrographs of fractured surfaces, MBS particles act as stress concentrators under tensile stress, which leads to the formation of holes within the cores of rubber particles when there is a strong interfacial bonding between the components and relatively weak strength of rubber phase itself.
4. The toughening-mechanism investigation revealed that shear yielding occurred in the PLA matrix as induced by the cavitation of MBS particles.
5. MBS could be used effectively as impact modifier of PLA.

References

1. Hiljanen-Vainio, M.; Varpomaa, P.; Seppala, J.; Tormala, P. Macromol Chem Phys 1996, 197, 1503.
2. Anderson, K. S.; Lim, S. H.; Hillmyer, M. A. J Appl Polym Sci 2003, 89, 3757.
3. Li, B. H.; Yang, M. C. Polym Adv Technol 2006, 17, 439.
4. Takagi, Y.; Yasuda, R.; Yamaoka, M.; Yamane, T. J Appl Polym Sci 2004, 93, 2363.
5. Li, T. N.; Turng, L. S. Polym Eng Sci 2006, 46, 1419.
6. Wang, R. Y.; Wang, S. F.; Zhang, Y.; Wan, C. Y.; Ma, P. M. Polym Eng Sci 2009, 49, 26.
7. Yuan, Y. M.; Ruckenstein, E. Polym Bull 1998, 40, 485.
8. Li, Y. J.; Shimizu, H. Macromol Biosci 2007, 7, 921.
9. Feng, F.; Ye, L. J Appl Polym Sci 2011, 119, 2778.
10. Han, J. J.; Huang, H. X. J Appl Polym Sci 2011, 120, 3217.
11. Liu, H. Z.; Zhang, J. W. J Polym Sci Part B: Polym Phys 2011, 49, 1051.
12. Zhang, X. C.; Goosen, M. F. A.; Wyss, U. P.; Pichora, D. J Macromol Sci Rev Macromol Chem Phys 1993, C33, 81.
13. Wu, S. Polymer 1985, 26, 1855.
14. Sultan, J. N.; McGarry, F. J. Polym Eng Sci 1973, 13, 29.
15. Borggreve, R. J. M.; Gaymans, R. J.; Eichenwald, H. M. Polymer 1985, 30, 78.
16. Lovell, P. A.; Mcdonald, J.; Saunders, D. E. J.; Young, R. J. Polymer 1993, 34, 61.
17. Bucknall, C. B. Toughened Plastics; Applied Sciences: London, 1977.
18. Kolarlk J.; Lednicky, F. Polym Eng Sci 1992, 32, 886.

19. Park, J. W.; Im, S. S. J Appl Polym Sci 2002, 86, 647.
20. Bhardwaj, R.; Mohanty, A. K. Biomacromolecules 2007, 8, 2476.
21. Zhang, G. B.; Zhang, J. M.; Wang, S. G.; Shen, D. Y. J Polym Sci Part B: Polym Phys 2003, 41, 23.
22. Si, Q. B.; Zhou, C.; Yang, H. D.; Zhang, H. X. Eur Polym J 2007, 43, 3060.
23. Crawford, E.; Lesser, A. J. Polymer 2000, 41, 5865.
24. Havriliak, S., Jr.; Slavin, S. E.; Shortridge, T. J. Polym Int 1991, 25, 67.
25. Havriliak, S., Jr.; Shortridge, T. J. J Polym Sci Part B: Polym Phys 1990, 28, 1987.
26. Fischer, E. W.; Sterzed, H. J.; Wegner, G. Colloid Polym Sci 1973, 251, 980.
27. Sarasua, J. R.; Prud'homme, R. E.; Wisniewski, M.; Borgne, A. L.; Spassky, N. Macromolecules 1998, 31, 3895.
28. Jiang, L.; Wolcott, M. P.; Zhang J. W. Biomacromolecules 2006, 7, 199.
29. Lazzeri, A.; Bucknall, C. B. J Mater Sci 1993, 28, 6799.
30. Paul, D. R.; Bucknall, C. B. Polymer 2009, 50, 5539.
31. Gaymans, R. J. In Polymer Blends; Paul, D. R., Bucknall, C. B., Eds.; Wiley: New York, 2000; Vol. 2.
32. Larocca, N. M.; Hage, E.; Pessan, L. A. Polymer 2004, 45, 5265.
33. Wu, G. F.; Zhang, J. F.; Shi, H. T.; Zhang, H. X. Eur Polym J 2004, 40, 2451.
34. Chang, S. Q.; Xie, T. X.; Yang, G. S. J Appl Polym Sci 2006, 102, 5184.
35. Premphet, K.; Preechachon, I. J Appl Polym Sci 2000, 76, 1929.
36. Muratoglu, O. K.; Argon, A. S.; Cohen, R. E.; Weinberg, M. Polymer 1995, 36, 921.
37. Barteczak, Z.; Argon, A. S.; Cohen, R. E.; Weinberg, M. Polymer 1999, 40, 2331.